

Evaluation of Photostationary and Non-Photostationary Operational Models for NOX Pollution in a Street Canyon

*Original*

Evaluation of Photostationary and Non-Photostationary Operational Models for NOX Pollution in a Street Canyon /  
Soulhac, L; Fellini, S; Nguyen, Cv; Salizzoni, P. - In: ATMOSPHERIC ENVIRONMENT. - ISSN 1352-2310. - 297:(2023),  
p. 119589. [10.1016/j.atmosenv.2023.119589]

*Availability:*

This version is available at: 11583/2978215 since: 2023-04-27T14:19:21Z

*Publisher:*

PERGAMON-ELSEVIER SCIENCE LTD

*Published*

DOI:10.1016/j.atmosenv.2023.119589

*Terms of use:*

This article is made available under terms and conditions as specified in the corresponding bibliographic description in the repository

*Publisher copyright*

Elsevier postprint/Author's Accepted Manuscript

© 2023. This manuscript version is made available under the CC-BY-NC-ND 4.0 license  
<http://creativecommons.org/licenses/by-nc-nd/4.0/>. The final authenticated version is available online at:  
<http://dx.doi.org/10.1016/j.atmosenv.2023.119589>

(Article begins on next page)

# Evaluation of photostationary and non-photostationary operational models for NO<sub>x</sub> pollution in a street canyon

L. Soulhac<sup>a</sup>, S. Fellini<sup>a</sup>, C.V. Nguyen<sup>b</sup>, P. Salizzoni<sup>b</sup>

<sup>a</sup>*Univ. Lyon, INSA Lyon, CNRS, Ecole Centrale de Lyon, Univ. Claude Bernard Lyon 1, LMFA, UMR5509, 69621, Villeurbanne France*

<sup>b</sup>*Univ. Lyon, Ecole Centrale de Lyon, CNRS, Univ. Claude Bernard Lyon 1, INSA Lyon, LMFA, UMR5509, 69130, Ecully, France*

---

---

## 1 Abstract

2 To predict pollutant concentration in urban areas, it is crucial to take into  
3 account the chemical transformations of reactive pollutants in operational dis-  
4 persion models. In this work, we derive and discuss two photostationary (with  
5 constant or varying transformation rates) and one non-photostationary chemi-  
6 cal models for NO – NO<sub>2</sub> – O<sub>3</sub> pollution in a street canyon. In the analytical  
7 derivation, we focus on the chemical and transport time scales to evaluate the  
8 applicability of the models in different urban contexts. We then assess their  
9 performance in predicting NO<sub>2</sub>, NO and O<sub>3</sub> concentration at three locations  
10 within an urban district by comparing the model predictions with measure-  
11 ments acquired in a field campaign. The results are in line with analytical  
12 speculations and highlight in which street types non-photostationary models  
13 can bring substantial advantages. In courtyards with limited ventilation and  
14 without direct emissions, the performance of the photostationary model with  
15 meteorology-based transformation rates is satisfactory. On the other hand, the  
16 application of a non-photostationary model significantly improves the predic-  
17 tions in urban canyons with direct vehicular emissions. The applicability of the  
18 proposed models in operational tools at the city scale is finally discussed.

19 **Keywords**

20 Photochemical smog, Urban air quality, Non-photostationary chemical model,  
21 Air pollution measurement campaign

22 **Introduction**

23 The time scales related to pollutant transfer over large urban agglomerations  
24 range from a few minutes to several hours. During this period, a large num-  
25 ber of physico-chemical processes take place and determine the concentration of  
26 pollutants in the urban atmosphere (Sillman, 1999). When the focus is on dis-  
27 persion at the local district scale, the rate of turbulent transport is considerably  
28 high compared to the rate of chemical transformation and most of the atmo-  
29 spheric compounds can be treated as inert tracers. There are however chemical  
30 reactions which are sufficiently fast to significantly affect the concentration of  
31 pollutants during their residence time in the streets. This is notably the case for  
32 nitrogen oxides. The nitrogen oxides that are most relevant for air pollution are  
33 generally indicated as  $\text{NO}_x$  and include nitrogen dioxide ( $\text{NO}_2$ ) and nitrogen  
34 monoxide ( $\text{NO}$ ).

35 The emissions of  $\text{NO}_x$  result from combustion processes, especially from  
36 motor vehicle engines or from power stations and industries. They are there-  
37 fore a tracer of anthropogenic activity in urban areas and their trends are used  
38 to assess the effectiveness of regulations on air pollution, or to evaluate the  
39 effects of sudden changes in emissions, such as during COVID-19 restrictions  
40 (e.g., Toscano and Murena, 2020; Lovarelli et al., 2020; Misra et al., 2021).  
41 It is generally assumed that the partition of  $\text{NO}_x$  at the point of emission is  
42 approximately between 10% to 15% for  $\text{NO}_2$  and 85% to 90% for  $\text{NO}$  (Ntzi-  
43 achristos et al., 2000). Acute exposure to  $\text{NO}_x$  causes respiratory disease and  
44 compromises lung functioning when inhaled at high concentrations. Children  
45 are the most vulnerable, with a demonstrated increased incidence of childhood  
46 asthma due to  $\text{NO}_2$  emissions from vehicular traffic (Khreis et al., 2017; Anen-  
47 berg et al., 2022). Despite being the major contributor to  $\text{NO}_x$ ,  $\text{NO}$  is less

48 toxic than  $\text{NO}_2$ . However, as most radicals, it is extremely unstable and forms  
49  $\text{NO}_2$  through photochemical oxidation. Nitrogen dioxide is then converted back  
50 to  $\text{NO}$  as a result of photolysis which also leads to the regeneration of ozone  
51 ( $\text{O}_3$ ). When the photostationary state is reached, these reactions result in a cy-  
52 cle with zero net chemistry and the chemical compounds reach the equilibrium  
53 composition, which can be easily derived in terms of kinetic reaction parame-  
54 ters by the Leighton relation (Leighton, 1961). Deviations from this state occur  
55 when (i) the residence time of pollutants in the reference volume (i.e. the street)  
56 is shorter than the time needed for reaching the photostationary equilibrium,  
57 (ii) turbulent motions mix the reactants so slowly that they remain segregated  
58 rather than reacting (Li et al., 2021), (iii) the transformation of nitrogen monox-  
59 ide into  $\text{NO}_2$  is altered by the role of complex reactions with radicals resulting  
60 from the oxidation of Volatile Organic Compounds (VOCs) and  $\text{CO}$  (Jenkin  
61 and Clemitshaw, 2000). The concentrations of  $\text{NO}$  and  $\text{NO}_2$  are also affected  
62 by reactions involving the hydroxyl radical and leading to the production of  
63 nitric acid.

64 The coupling of turbulent and chemical dynamics to assess photochemi-  
65 cal pollution in urban areas has been explored extensively in the past two  
66 decades by means of Computational Fluid Dynamics (CFD) simulations. Baker  
67 et al. (2004) extended a Large Eddy Simulation (LES) for turbulent flow in  
68 a street canyon with a simple  $\text{NO}_x\text{-O}_3$  chemical model. The same reaction  
69 scheme was adopted by Baik et al. (2007), who instead used Reynolds-averaged  
70 Navier–Stokes (RANS) simulations. By introducing a photostationary state de-  
71 fect index, both studies highlighted the regions of a street canyon most prone  
72 to chemical instability. The chemistry of VOC has been included in RANS sim-  
73 ulations by Kwak and Baik (2012) and Kim et al. (2012), while Bright et al.  
74 (2013) combined LES simulations with a detailed chemical reaction mechanism  
75 (Reduced Chemical Scheme) comprising 51 chemical species and 136 reactions.  
76 Similarly, Garmory et al. (2009) used the Stochastic Fields (FS) method to sim-  
77 ulate turbulent reacting flows with a chemistry model comprising 28 species.  
78 These studies showed that the effect of turbulent fluctuations (i.e. segregation)

79 on the chemistry is significant for species with the highest transformation rates.  
80 They also showed that increasing chemical complexity (i.e. simulating VOC  
81 chemistry) could contribute to additional but modest  $\text{NO}_2$  and  $\text{O}_3$  formation in  
82 the canyon.

83 CFD simulations, coupled with detailed chemical models, provide an accu-  
84 rate prediction but are computationally expensive and require a large amount of  
85 detailed input data. To simulate air quality in large urban domains, consisting  
86 of hundreds to thousands of streets, a more efficient way is adopting simplified  
87 modelling approaches (Vardoulakis et al., 2007). These are usually Gaussian-  
88 Lagrangian models integrated with box models to simulate the concentration in  
89 the street canyons. In these operational tools, photostationarity is a convenient  
90 assumption as it allows the modelling of  $\text{O}_3$  and  $\text{NO}_x$  as inert tracers and to  
91 subsequently apply photochemical equilibrium in the streets. This is the case of  
92 the Canyon Plume Box Model (CPBM) (Yamartino and Wiegand, 1986), and  
93 the street network model Sirane (Soulhac et al., 2017).

94 Another widespread approach is the adoption of empirical models to esti-  
95 mate  $\text{NO}$ - $\text{NO}_2$  conversion (Ravina et al., 2022). These are based on a photosta-  
96 tionary assumption but are optimised to fit observed concentrations. Hirtl and  
97 Baumann-Stanzer (2007) investigated the performances of the two empirical  
98 conversion schemes after Romberg et al. (1996) and after Derwent and Middle-  
99 ton (1996), when implemented in the Gaussian model Atmospheric Dispersion  
100 Modelling System (ADMS) and in the Lagrangian Simulation of Aerosol Trans-  
101 port (LASAT) model. These dispersion models turned out to be quite successful  
102 in predicting average concentrations measured in street canyons.

103 A step forward in modeling the interaction between the time scales of chem-  
104 ical reactions and those of transport is represented by the model ADMS-Urban  
105 (McHugh et al., 1997; Carruthers et al., 2000). In ADMS-Urban,  $\text{NO}_x$  chem-  
106 istry can be modelled by the Generic Reaction Set (GRS) (Azzi et al., 1992;  
107 Venkatram et al., 1994) photochemical scheme which includes seven chemical  
108 reactions. The GRS chemical model is applied to the emitted pollutants after  
109 transport and dispersion. The chemistry calculation for the receptor is split in

110 two steps: the first considers the contribution from far sources (source-receptor  
111 travel time greater than 150 s), while the second one includes the contribution  
112 from the nearest sources (source-receptor travel time less than 150 s) (CERC,  
113 2022). In this way, the model takes into account the travel time of the pollution  
114 plume and it assumes a time -or distance- dependence on the generation of NO<sub>2</sub>.

115 Finally, the Operational Street Pollution Model (OSPM) (Palmgren et al.,  
116 1996; Berkowicz et al., 1997) is a street canyon model which includes NO –  
117 NO<sub>2</sub> – O<sub>3</sub> chemistry by means of a non-photostationary model that takes into  
118 account the interaction between the chemical reaction rates and the residence  
119 time of the pollutants in the street.

120 The overview above suggests that operational modeling of reactive pollu-  
121 tant concentration at the urban scale requires an adequate description of (i) the  
122 chemistry, (ii) the turbulent transport, (iii) the interaction between these two  
123 processes, all while minimizing the computational cost and required input data  
124 in order to be applied to hundreds to thousands of streets. To date, empirical  
125 relationships and photostationary models are the most commonly used for op-  
126 erational purposes while non-photostationary schemes are rarely implemented.  
127 This is especially true for street network models, where, to our knowledge, the  
128 non-photostationary scheme has not yet been implemented. Furthermore, the  
129 existing literature lacks a coherent formulation of the different photochemical  
130 models, with a clear statement of the underlying assumptions and a concurrent  
131 validation with real data. To fill these gaps, in this work, we derive, com-  
132 pare and validate three models for NO<sub>X</sub> photochemical pollution that can be  
133 efficiently implemented in street network models at the city scale. In the ana-  
134 lytical derivation, we focus on the time scales of pollutant transformation and  
135 transport in order to highlight the range of application of the different models.  
136 To verify the reliability of the different schemes we compare the model outputs  
137 to field data. The main objective is to evaluate whether the application of a  
138 non-photostationary model can bring substantial advantages in the prediction of  
139 pollutant concentration in the streets, with respect to photostationary models.

140 The formulation of a photochemical model, adopting box-model approach,

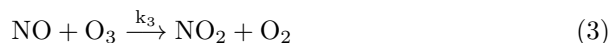
141 is presented in 1. A general presentation of the measurement campaign is given  
142 in Section 2. Results are discussed in Section 3, while the conclusions are drawn  
143 in Section 4.

## 144 1. NO – NO<sub>2</sub> – O<sub>3</sub> chemical street model

145 To maximize computational efficiency, minimize input data while providing  
146 a satisfactory description of pollution in the urban area, city-scale operational  
147 models, such as street network models (Soulhac et al., 2011), generally provide a  
148 single concentration value for each street. This can be notably achieved adopt-  
149 ing a box model at the street scale, which provides spatially averaged pollutant  
150 concentration by computing a pollutant budget over the volume of the street. In  
151 order to simulate photochemical pollution, the pollutant budget has to take into  
152 account the terms of chemical production and of chemical destruction (Soulhac  
153 et al., 2011) as well as those related to the turbulent fluxes at the street edges  
154 and at the top of the street.

155

156 To write the budget of photochemical pollutants in the street, we start by  
157 considering the simplified chemical scheme involving NO, NO<sub>2</sub> and O<sub>3</sub>:



158 It is known (Seinfeld, 1986) that the second equation is much faster than  
159 the first and the third ones, so that the constants  $k_1$  and  $k_3$  are the limiting  
160 parameters of these chemical reactions. The constant rate  $k_1$  (NO<sub>2</sub> photolysis  
161 rate) depends on the intensity of solar radiation, whilst  $k_3$  depends on air tem-  
162 perature. These dependences can be modeled by the following relations (Kasten  
163 and Czeplak, 1980; Seinfeld, 1986):

$$\begin{cases} k_1 = \frac{1}{60}(0.5699 - [9.056 \cdot 10^{-3}(90 - \zeta)]^{2.546}) \left(1 - 0.75 \left[\frac{Cld}{8}\right]^{3.4}\right) (\text{s}^{-1}) \\ k_3 = 1.325 \cdot 10^6 \exp\left(-\frac{1430}{T}\right) (\text{m}^3\text{mol}^{-1}\text{s}^{-1}) \end{cases} \quad (4)$$

164 where  $\zeta$  is the solar elevation in degrees,  $T$  is the air temperature in Kelvin  
165 and  $Cld$  is the cloud coverage in Oktas. These meteorological parameters vary  
166 over time. In operational dispersion models, the time-dependence of the mete-  
167 orological parameter is usually modelled assuming a quasi-steady approach, i.e.  
168 assuming steady condition of time step of 1 hours. Cloud coverage and temper-  
169 ature are measured during the day at meteorological stations, while the solar  
170 elevation is a function of the day of the year, the local hour and the site latitude  
171 (e.g., Soulhac et al., 2011). Note that  $k_1$  is set equal to 0 at night, when the  
172 solar elevation angle is negative. More sophisticated models for  $k_1$  and  $k_3$  are  
173 available in the literature, but they are generally not adapted for operational  
174 purposes (Seinfeld, 1986).

175 Referring to Eqs. 1-3, the production and destruction terms for each chem-  
176 ical species are related to the molar concentration by the following expressions:

$$\begin{aligned} P_{NO} &= k_1[\text{NO}_2] & D_{NO} &= k_3[\text{NO}][\text{O}_3] \\ P_{NO_2} &= k_3[\text{NO}][\text{O}_3] & D_{NO_2} &= k_1[\text{NO}_2] \\ P_{O_3} &= k_1[\text{NO}_2] & D_{O_3} &= k_3[\text{NO}][\text{O}_3] \end{aligned} \quad (5)$$

177 where  $[\cdot]$  represents the molar concentration ( $\text{mol}/\text{m}^3$ ) of the compound.

178

179 We include the production and destruction terms in the street box model  
180 formulated in Soulhac et al. (2011). Neglecting wet and dry deposition phenom-  
181 ena, the budget of time-averaged concentration of  $\text{NO}_2$ ,  $\text{NO}$  and  $\text{O}_3$  for a single  
182 street-canyon of length  $L$ , width  $W$  and height  $H$ , can be written:

$$Q_{\text{NO}_2} - u_d \mathcal{S}_h ([\text{NO}_2] - [\text{NO}_2]^\dagger) - U \mathcal{S}_v ([\text{NO}_2] - [\text{NO}_2]^\dagger) + k_3 [\text{NO}][\text{O}_3] \mathcal{V} - k_1 [\text{NO}_2] \mathcal{V} = 0 \quad (6)$$

183

$$Q_{\text{NO}} - u_d \mathcal{S}_h ([\text{NO}] - [\text{NO}]^{\text{f}}) - U \mathcal{S}_v ([\text{NO}] - [\text{NO}]^{\text{f}}) + k_1 [\text{NO}_2] \mathcal{V} - k_3 [\text{NO}] [\text{O}_3] \mathcal{V} = 0 \quad (7)$$

184

$$-u_d \mathcal{S}_h ([\text{O}_3] - [\text{O}_3]^{\text{f}}) - U \mathcal{S}_v ([\text{O}_3] - [\text{O}_3]^{\text{f}}) + k_1 [\text{NO}_2] \mathcal{V} - k_3 [\text{NO}] [\text{O}_3] \mathcal{V} = 0 \quad (8)$$

185

186

187

188

189

190

191

192

193

194

195

196

where  $\mathcal{V} = LWH$  is the volume of the street,  $\mathcal{S}_h = LW$  is its horizontal area and  $\mathcal{S}_v = WH$  is its vertical cross section. The velocities  $U$  and  $u_d$  are the mean velocity along the street and the exchange rate at roof level (e.g., Soulhac et al., 2008; Salizzoni et al., 2009; Fellini et al., 2020) and they drive the longitudinal and vertical pollutant fluxes entering and leaving the street volume. For each of the three chemical compounds  $\text{NO}_2$ ,  $\text{NO}$  and  $\text{O}_3$ ,  $Q$  is the molar emission in the street,  $[\cdot]^{\text{f}}$  is the concentration in the atmosphere above roofs, and  $[\cdot]$  is the concentration in the flow advected within the canopy at the upwind intersection of the street. We point out that the source of ozone is not included in the budget (i.e.  $Q_{\text{O}_3} = 0$ ) since direct ozone emissions in the streets are rare. Eqs. 6-8 can be reformulated by highlighting the time scales associated with the terms of transport and chemical reaction. For example, for  $\text{NO}_2$  we can write:

$$\frac{Q_{\text{NO}_2}}{\mathcal{V}} - \frac{[\text{NO}_2] - [\text{NO}_2]^{\text{f}}}{\tau_v} - \frac{[\text{NO}_2] - [\text{NO}_2]^{\text{f}}}{\tau_h} + \frac{[\text{NO}]}{\tau_3} - \frac{[\text{NO}_2]}{\tau_1} = 0 \quad (9)$$

197 with

$$\begin{cases} \tau_v = \frac{H}{u_d} \\ \tau_h = \frac{L}{U} \\ \tau_1 = \frac{1}{k_1} \\ \tau_3 = \frac{1}{k_3[\text{O}_3]} \end{cases} \quad (10)$$

198

199

200

201

202

203

204

To determine the order of magnitude of the different terms in Eq. 9 we can roughly estimate the time scales involved, based on the data collected and simulated for the city of Lyon (France) (Soulhac and Salizzoni, 2010; Soulhac et al., 2012). The depth  $H$  and length  $L$  of street canyons vary in the ranges 15-30 m and 20-150 m, respectively. The wind speed within the streets  $U$  and the typical turbulent exchange velocity  $u_d$  can reasonably be assumed in the ranges 0.1-5 m/s and 0.01-0.22 m/s, respectively (Salizzoni et al., 2009; Soulhac et al.,

205 2011) when the free stream wind above the city is between 1.5 m/s and 8 m/s  
 206 (Météo-France data for the period 1981–2006) From these data, we obtain that  
 207  $\tau_v$  ranges in 68-3000 s, and  $\tau_h$  in 4-1500 s. Typical values of  $k_1$  and  $k_3$  can be  
 208 estimated by means of Eq. 4 by varying the cloud coverage  $Cld$  between 0 and  
 209 8, the temperature  $T$  in 5°C-30°C and  $\zeta$  in 10°-90° (in this analysis we consider  
 210 only daytime). The concentration of ozone can be taken in the range 25-75 ppb  
 211 (data measured at Saint-Exupery station for the year 2008). These data provide  
 212  $\tau_1$  in the range 105-1850 s and  $\tau_3$  in the range 54-247 s. Moreover, we introduce  
 213 an average time scale  $\tau_s$  related to the pollutant wash-out from the street:

$$\tau_s = \left( \frac{1}{\tau_h} + \frac{1}{\tau_v} \right)^{-1} \quad (11)$$

214 and we find that  $\tau_s$  varies approximately in the range 4-1000 s. This analysis  
 215 shows that there is an overlap between the timescales associated to chemical  
 216 reactions and the characteristic residence times of pollutants within the street.  
 217 Consequently a modeling approach combining chemistry and advection-diffusion  
 218 processes must be adopted, as neither of the two processes can be neglected.

219

220 Finally, we define the average background concentration  $[\cdot]^b$  as:

$$[\cdot]^b = \frac{\frac{[\cdot]^c}{\tau_h} + \frac{[\cdot]^r}{\tau_v}}{\frac{1}{\tau_h} + \frac{1}{\tau_v}} \quad (12)$$

221 .

222 In this way, Eq. 9 can be simplified using only the background concentration  
 223  $[\text{NO}_2]^b$ :

$$\frac{Q_{\text{NO}_2}}{\mathcal{V}} - \frac{[\text{NO}_2] - [\text{NO}_2]^b}{\tau_s} + k_3[\text{NO}][\text{O}_3] - k_1[\text{NO}_2] = 0 \quad (13)$$

224 The same formulation is valid for NO and O<sub>3</sub> so that a system of 3 equations  
 225 (Eq. 13 and the two analogous balances for NO and O<sub>3</sub>) describes in a compact  
 226 way the dynamics of the three chemical compounds. In what follows, we will  
 227 examine the solution of this system of equations adopting different scenarios  
 228 related to the relative importance of the different time scales involved.

229 *1.1. Passive scenario*

230 As a first step, we consider the case of a passive pollutant, whose concentra-  
 231 tion is generally referred to as  $[\cdot]^*$ . For  $\text{NO}_2$  Eq. 13 simplifies as:

$$\frac{Q_{\text{NO}_2}}{\mathcal{V}} - \frac{[\text{NO}_2]^* - [\text{NO}_2]^b}{\tau_s} = 0. \quad (14)$$

232 This scenario corresponds to the case of reaction times that are extremely long  
 233 (i.e.  $\tau_1 \rightarrow \infty$ ,  $\tau_3 \rightarrow \infty$ ) so that the terms of chemical production and destruction  
 234 are negligible for the budget in the street. The solution is given by:

$$[\text{NO}_2]^* = [\text{NO}_2]^b + \frac{\tau_s Q_{\text{NO}_2}}{\mathcal{V}} \quad (15)$$

235 By analogy, the relative solution for the ‘passive’ NO concentration reads:

$$[\text{NO}]^* = [\text{NO}]^b + \frac{\tau_s Q_{\text{NO}}}{\mathcal{V}} \quad (16)$$

236 and for  $\text{O}_3$  concentration, assuming no emission of ozone:

$$[\text{O}_3]^* = [\text{O}_3]^b. \quad (17)$$

237 The concentration  $[\cdot]^*$  takes into account all contributions to pollution de-  
 238 riving from advective transport only, i.e. the direct emission into the street and  
 239 the transport of pollutants to the street both from adjacent street and from the  
 240 atmosphere above the roofs. Thus, Eqs. 15-17 can be seen as the general solu-  
 241 tions for a dispersion model able to provide passively advected concentrations  
 242 in the streets.

243 *1.2. Photostationary chemical model*

244 Let us now consider that the reactive pollutants in the control volume (i.e.  
 245 within the street canyon) have the necessary time to reach the photochemical  
 246 equilibrium. This corresponds to assume that the characteristic time scales of  
 247 the chemical reactions  $\tau_1$  and  $\tau_3$  are small compared to the residence time of  
 248 pollutants within the street (i.e.  $\tau_1$  and  $\tau_3 \rightarrow 0$ ). Under these assumptions,  
 249 the advective and source terms in Eq. 13 become negligible compared to the

250 production and destruction terms and the balance equation is simplified as fol-  
 251 lows:

$$k_3[\text{NO}]^\infty[\text{O}_3]^\infty - k_1[\text{NO}_2]^\infty = 0 \quad (18)$$

252 where the photostationary concentrations have been referred to as  $[\cdot]^\infty$ . Eq. 18  
 253 is known as the Leighton relationship (Leighton, 1961), whose formulation could  
 254 also be obtained from the budget of  $\text{NO}_2$  or  $\text{O}_3$  (see Eqs. 7 and 8).

255 The conservation of N and O species lead to the following relations, which  
 256 are valid for passive, photostationary or non-photostationary concentrations:

$$[\text{NO}] + [\text{NO}_2] = [\text{NO}]^* + [\text{NO}_2]^* = [\text{NO}]^\infty + [\text{NO}_2]^\infty = \phi_N, \quad (19)$$

$$[\text{O}_3] + [\text{NO}_2] = [\text{O}_3]^* + [\text{NO}_2]^* = [\text{O}_3]^\infty + [\text{NO}_2]^\infty = \phi_O, \quad (20)$$

257 where  $\phi_N$  and  $\phi_O$  are constants defining the proportion of the different species,  
 258 whatever the chemical history of the pollutants reaching the street canyon. We  
 259 note that  $\phi_N$  and  $\phi_O$  can be easily computed from the results of the passive  
 260 model providing the concentrations  $[\cdot]^*$  (Section 1.1) which take into account  
 261 all the pollutant contributions reaching the canyon (i.e. both direct emissions  
 262 and transported pollutants).

263 Combining Eqs. 18 to 20 (see e.g., Soulhac et al. (2011)) provides the solu-  
 264 tion:

$$[\text{NO}_2]^\infty = \frac{b - \sqrt{b^2 - 4c}}{2} \quad (21)$$

265 with:

$$\begin{cases} b = \frac{k_1}{k_3} + [\text{O}_3]^* + [\text{NO}]^* + 2[\text{NO}_2]^* = \frac{k_1}{k_3} + \phi_N + \phi_O \\ c = ([\text{O}_3]^* + [\text{NO}_2]^*) ([\text{NO}]^* + [\text{NO}_2]^*) = \phi_O \cdot \phi_N \end{cases} \quad (22)$$

266 Eq. 22 illustrates that  $\text{NO}_2$  concentration depends only on  $k_1/k_3$ ,  $\phi_N$  and  
 267  $\phi_O$ . This highlights that the chemical history of the background concentration,  
 268 that is included in passive concentrations  $[\cdot]^*$  by equations 15 to 17, has no

269 influence on the photostationary solution because this solution corresponds to  
 270 an infinite reaction time, which offsets the initial repartition between NO, NO<sub>2</sub>  
 271 and O<sub>3</sub>.

272 Once [NO<sub>2</sub>]<sup>∞</sup> is known, Eqs. 19 and 20 provide [NO]<sup>∞</sup> and [O<sub>3</sub>]<sup>∞</sup>.

### 273 1.3. Non-photostationary chemical model

274 To find the general solution for the full chemical street model (Eq.13), we  
 275 take the difference between Eqs. 13 and 14:

$$-\frac{[\text{NO}_2] - [\text{NO}_2]^*}{\tau_s} + k_3[\text{NO}][\text{O}_3] - k_1[\text{NO}_2] = 0 \quad (23)$$

276 By introducing Eqs. 19 and 20 in Eq. 23:

$$-\frac{[\text{NO}_2] - [\text{NO}_2]^*}{\tau_s} + k_3([\text{NO}]^* + [\text{NO}_2]^* - [\text{NO}_2])([\text{O}_3]^* + [\text{NO}_2]^* - [\text{NO}_2]) - k_1[\text{NO}_2] = 0 \quad (24)$$

277 and rearranging, the equation for [NO<sub>2</sub>] is finally:

$$[\text{NO}_2]^2 - b'[\text{NO}_2] + c' = 0 \quad (25)$$

278 with

$$\begin{cases} b' = b + \frac{1}{k_3\tau_s} \\ c' = c + \frac{[\text{NO}_2]^*}{k_3\tau_s} \end{cases} \quad (26)$$

279 We obtain the non-photostationary solution for [NO<sub>2</sub>] is then:

$$[\text{NO}_2] = \frac{b' - \sqrt{b'^2 - 4c'}}{2} \quad (27)$$

280 This expression is very similar to the photo-chemical model implemented in  
 281 OSPM (Palmgren et al., 1996; Berkowicz et al., 1997) but generalized for a  
 282 street canyon with a longitudinal advection velocity  $U$  and a vertical turbulent  
 283 exchange rate  $u_d$ , therefore suitable for implementation in street network mod-  
 284 els. Also in this case, once [NO<sub>2</sub>] is known, Eqs. 19 and 20 provide [NO] and  
 285 [O<sub>3</sub>].

286 The solution in Eqs. 26-27 can be discussed according to the asymptotic  
 287 values for the street residence time scale  $\tau_s$ , as shown in Fig. 1. If  $\tau_s \rightarrow 0$  (i.e.

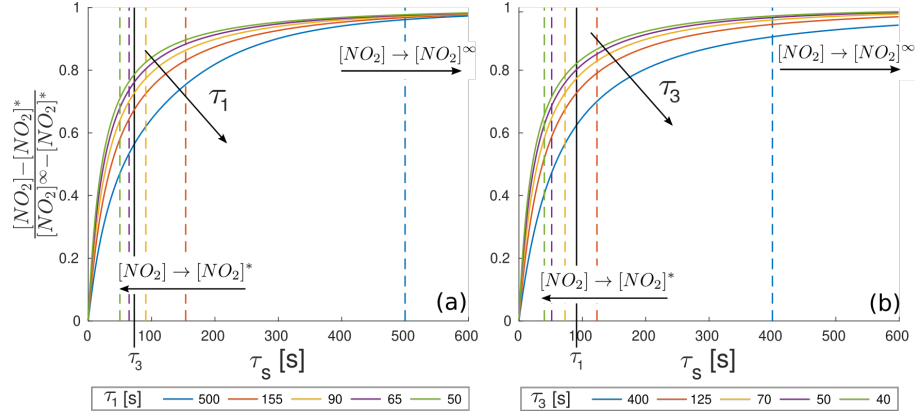


Figure 1: Trend of the non-photostationary solution ( $[NO_2]$ ) towards the solution for the passive model ( $[NO_2]^*$ ) and towards the photostationary solution ( $[NO_2]^\infty$ ) as a function of the characteristic time of advective transport ( $\tau_s$ ), and of the two characteristic times of reaction. Panel (a) shows different curves as a function of  $\tau_1$ , indicated in the legend and by the dashed vertical lines. Similarly, panel (b) shows the curves as a function of  $\tau_3$  indicated in the legend and by the dashed vertical lines.

288  $\tau_s \ll \tau_1$  and  $\tau_3$ ), according to Eq. 24, we have that  $[NO_2] \rightarrow [NO_2]^*$ . It means  
 289 that the pollutants have no time to react and the concentration of the chemical  
 290 species is provided by the passive solution (Eqs. 15-17). On the other hand, if  
 291  $\tau_s$  tends to infinity (i.e.  $\tau_s \gg \tau_1$  and  $\tau_3$ ), then  $b = b'$  and  $c = c'$  in Eq. 26 and  
 292 the concentration  $[NO_2]$  tends to  $[NO_2]^\infty$ . It means that the pollutants have  
 293 an infinite time to react and the final concentration of the chemical species is  
 294 provided by the photostationary solution (Eq. 21).

295 For intermediate values of  $\tau_s$ , the solution is in-between, with only a partial  
 296 conversion from NO to  $NO_2$ , compared to the photostationary limit. We can  
 297 remark that, unlike the photostationary case, Eq. 26 includes  $[NO_2]^*$  independ-  
 298 dently of the constants  $\phi_N$  and  $\phi_O$ . This adds a dependence of the solution on  
 299 the chemical history of the background concentration.

300

301 To provide further interpretations, Eq. 24 can be rewritten in the form:

$$\underbrace{[NO_2]^*}_{\alpha} \chi^2 - \underbrace{\left( \frac{k_1}{k_3} + [O_3]^* + [NO]^* + \frac{1}{k_3 \tau_s} \right)}_{\beta} \chi + \underbrace{\left( \frac{[NO]^* [O_3]^*}{[NO_2]^*} - \frac{k_1}{k_3} \right)}_{\gamma} = 0 \quad (28)$$

302 with

$$\chi = \frac{[\text{NO}_2] - [\text{NO}_2]^*}{[\text{NO}_2]^*} = \frac{\beta - \sqrt{\beta^2 - 4\alpha\gamma}}{2\alpha}. \quad (29)$$

303 where  $\chi$  represents the rate of increase of  $\text{NO}_2$  concentration with respect to  
304 its passive value  $[\text{NO}_2]^*$ . The term  $\gamma$  can be seen as a quantification of the  
305 non-photostationarity of the passive concentrations of  $\text{NO}$ ,  $\text{NO}_2$  and  $\text{O}_3$ . Con-  
306 sequently, if the passive concentrations are already close to the photostationary  
307 equilibrium ( $\gamma \simeq 0$ ), then the solution tends to  $\chi \simeq 0$ , which means that the  
308 final concentration is close to the passive one.

309

#### 310 1.4. Validation strategy

311 As a further step, we test the analytical solutions presented in the previous  
312 sections against field data. In doing so, we will consider three different mod-  
313 els: the first one (Model 1) is the photostationary model (Eq. 21) where the  
314 transformation rates  $k_1$  and  $k_3$  are assumed to be constant with time, what-  
315 ever the temperature and radiative conditions. This solution can be adopted  
316 when the meteorological information (temperature, intensity of solar radiation)  
317 is missing and to minimize the computational cost. The sensitivity of the model  
318 to the value adopted for the  $k_1/k_3$  ratio is discussed in the following section.  
319 The second one (Model 2) is a photostationary model with transformation rates  
320 that vary during the day according to the meteorological conditions. To this  
321 aim, Eq. 4 is applied to estimate  $k_1$  and  $k_3$  with the parameters  $T$ ,  $Cld$  and  
322  $\zeta$  varying over the day. The third one (Model 3) is the model derived for the  
323 non-photostationary conditions in Eq. 27, with parameters  $k_1$  and  $k_3$  again  
324 varying during the day.

325 The models presented in sections 1.2 and 1.3 are designed to apply the chem-  
326 ical scheme (Eqs. 1-3) as a post-calculation after the application of a transport  
327 and dispersion model able to provide the advected concentrations in the street,  
328 i.e.  $[\text{NO}]^*$ ,  $[\text{NO}_2]^*$ , and  $[\text{O}_3]^*$ . In order to validate only the chemical models,  
329 avoiding the influence of errors due to the dispersion simulation, we have con-  
330 sidered a virtual perfect dispersion model by using the measured concentrations

331 in the streets as input data for the chemical models. According to Eqs. 21  
332 and 27, the results of the photochemical models depend on  $k_1/k_3$ ,  $\phi_N$ ,  $\phi_O$  and  
333  $[\text{NO}_2]^*$ . As mentioned above, the ratio  $k_1/k_3$  can be taken as a constant or  
334 estimated from meteorological data and as a function of time. Equations 19  
335 and 20 show that the conserved quantities  $\phi_N$  and  $\phi_O$  can be computed directly  
336 from the measured concentrations at the monitoring stations, which correspond  
337 to  $[\text{NO}]$ ,  $[\text{NO}_2]$ , and  $[\text{O}_3]$ . Once  $\phi_O$  is known,  $[\text{NO}_2]^*$  results from Eq. 20 by  
338 subtracting the measured background concentration of ozone (see Eq. 17). The  
339 other parameter of the non-photostationary model is the time scale  $\tau_s$ . In the  
340 validation, this parameter was adjusted to optimize the correlation coefficient  
341 between the model and measured concentrations. The resulting values will be  
342 discussed in the following section.

## 343 2. On-site measurements

344 The field data were measured during the LYON6 campaign which took  
345 place between the 9th and the 24th July 2001 in the 6th arrondissement in  
346 Lyon (France) and was handled by COPARLY (Comité de Coordination pour  
347 le contrôle de la Pollution Atmosphérique), the local authority for traffic and air  
348 pollution management, in collaboration with the Fluid Mechanics and Acous-  
349 tics Laboratory (LMFA) in École Centrale de Lyon. The campaign consisted of  
350 local measurements of vehicular traffic, air pollution and weather conditions.

351 The meteorological data were collected by two stations within the urban area  
352 (Fig. 2) and by a third one located 7 km from the studied district, and positioned  
353 away from any building that could directly influence the measurements. To have  
354 a representative dataset over the study district, the measurements from the  
355 three different stations were combined together. The reference temperature was  
356 measured by the sensors located within the urban area. To avoid local effects,  
357 cloud cover, precipitation, wind speed and wind direction were provided by the  
358 station outside the urban area. However, a correction to the wind intensity to  
359 take into account the difference in surface roughness was applied as detailed in

360 Soulhac et al. (2012). The temporal evolution of the resulting meteorological  
361 dataset is represented in Fig. 3.

362 Hourly concentration of nitrogen monoxide, nitrogen dioxide and ozone were  
363 measured by three monitoring stations, referred to as ‘Station 1’, ‘Station 2’ and  
364 ‘Station 3’. Station 1 was located in a busy street canyon. Station 2 and Station  
365 3 were located inside school courtyards, far away from polluting source. In this  
366 regard, we point out that the models derived in Section 1 are valid for both  
367 street canyons and urban courtyards as the fundamental assumption underlying  
368 the box model (Eq. 6-8) is the decoupling between the dynamics in the street  
369 and the dynamics above the roofs (Salizzoni et al., 2011). The urban courtyard  
370 differs from the street canyon by the absence of direct emissions and street  
371 intersections at the ends. For courtyards, therefore, the wash-out time scale  $\tau_s$   
372 (Eq. 11) corresponds to the rate of vertical exchange at roof level ( $\tau_h$ ) and  $Q_{NO}$   
373 and  $Q_{NO_2}$  are equal to zero.

374 In Station 2 and 3, the analyzers were placed at 2 m from the ground and  
375 in the middle of the courtyard. The concentration was measured over approxi-  
376 mately 6 days (see Fig. 3). In Station 1, the analyzer was also placed 2 m off  
377 the ground but a few centimeters from a building wall, and the concentration  
378 was measured over 15 days. In real street canyons there are several factors  
379 (e.g., traffic, vegetation, building geometries) that increase the mixing of pol-  
380 lutants therefore inducing a concentration field that is more homogeneous than  
381 that observed in controlled case studies in wind tunnels and numerical simula-  
382 tions, where a highly spatially inhomogeneous concentration field is predicted  
383 (Buccolieri et al., 2009; Marucci and Carpentieri, 2019; Fellini et al., 2020). For  
384 this reason, and considering that the focus of the proposed models is on hourly  
385 averaged pollution, the concentration in the canyon can be assumed sufficiently  
386 homogeneous and therefore less sensitive to the positioning of the sensor within  
387 the street. This is in line with previous validation studies of street network  
388 models (Soulhac et al., 2012, 2017) in which an influence of the sensor position  
389 on the agreement between the model and the measurements was not observed.

390 To estimate the concentration levels of background pollutants, other three

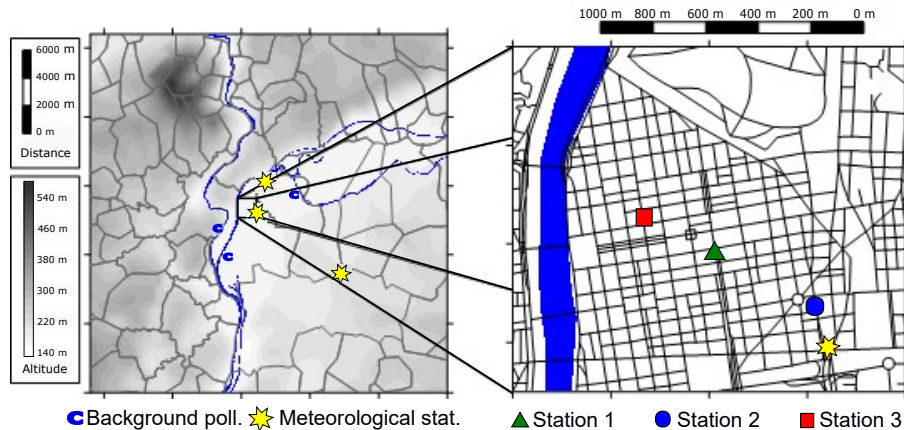


Figure 2: Location of the three meteorological stations, of the suburban stations for measuring pollution background and of the three pollution monitoring stations inside the study district.

391 monitoring stations located outside the district were used. Refer to Soulhac et al.  
 392 (2012) for a complete description of the measurement campaign and simulation  
 393 set-up.

### 394 3. Results

395 The meteorological data collected during the field campaign directly provide  
 396 the temporal evolution of the ratio  $k_1/k_3$ , estimated using Eq. 4. As shown  
 397 in Fig. 4-a, this ratio is far from being constant with time, and varies from a  
 398 maximum of about  $0.9 \mu\text{mol}/\text{m}^3$  (20 ppb) and a minimum close to 0 during  
 399 the night, with an average value of  $0.3 \mu\text{mol}/\text{m}^3$  (6.8 ppb). This is due to  
 400 the variation over time of temperature, cloud coverage and solar elevation (see  
 401 Eq. 4). As stated in Eq. 18, this ratio equals the ratio  $[\text{NO}][\text{O}_3]/[\text{NO}_2]$  when  
 402 the pollutants are in photostationary equilibrium. By using the measurements  
 403 from the three pollution monitoring stations, we test this condition in Fig. 4-  
 404 b and c. As usual in practical applications, concentration measurements are  
 405 provided also in ppb ( $C_x$  is the concentration in ppb of the chemical compound  
 406 x, while  $[x]$  is the molar concentration. The relation between the two is given  
 407 by the molar volume  $V_m$ , i.e.  $C_x = [x]V_m 10^9$ ). Results show that, for Station  
 408 2 and Station 3, the ratio  $[\text{NO}][\text{O}_3]/[\text{NO}_2]$  agrees well with the trend of the

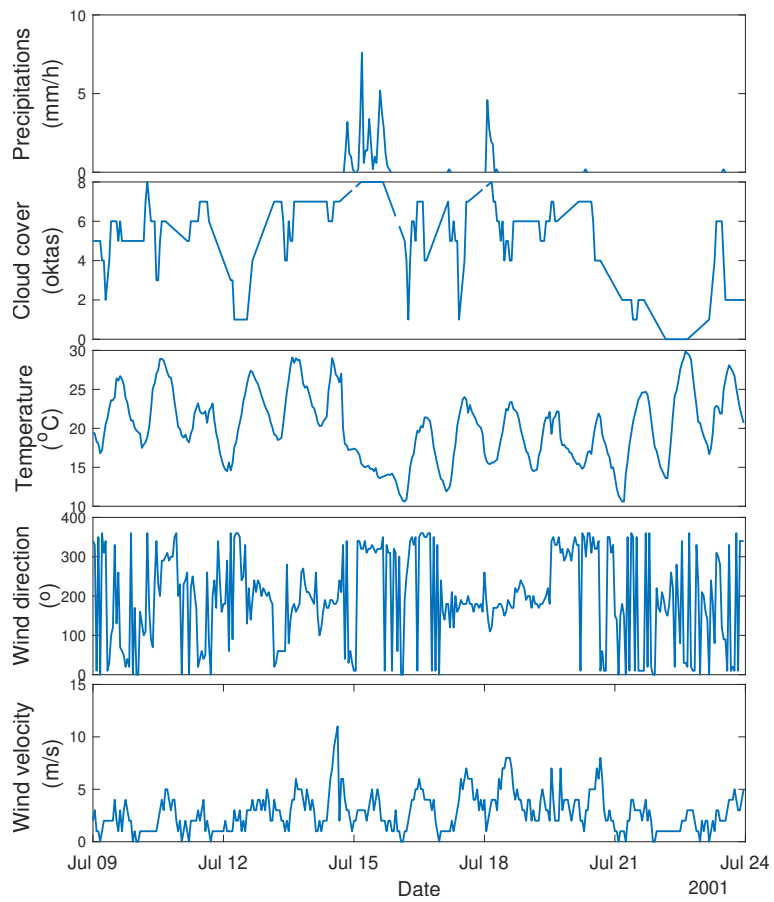


Figure 3: Temporal evolution of the meteorological parameters for the two-weeks campaign obtained by integrating the data from the different meteorological stations.

409 ratio  $k_1/k_3$ . This is in line with the analysis performed in Fig. 1: in sites  
 410 sheltered from direct vehicular emissions and with long residence times, the  
 411 photostationary equilibrium (Eq. 18) is a reliable assumption. Conversely, for  
 412 the busy street canyon (Station 1), the ratio  $[\text{NO}][\text{O}_3]/[\text{NO}_2]$  is generally higher  
 413 than  $k_1/k_3$  (Fig. 4-c). This is due to the fact that, at the emission,  $[\text{NO}_X]$   
 414 are mainly constituted by NO, that is progressively transformed in  $\text{NO}_2$  until  
 415 photostationary equilibrium is reached. For this reason, close to the source the  
 416 ratio  $[\text{NO}][\text{O}_3]/[\text{NO}_2]$  is expected to be higher than that corresponding to the  
 417 equilibrium.

418 This first analysis shows that the photostationary model has some limita-  
 419 tions when applied to busy street canyons with direct vehicular emissions.

420

421 To clarify this point, we assess the performance of the three photochemical  
 422 models (derived in Section 1 and retrieved in Section 1.4) in predicting the  
 423 concentration of  $[\text{NO}_2]$  in the three measurement stations. For the sake of  
 424 comparison, we include in our analysis the empirical model developed by Dixon  
 425 et al. (2001). Starting from the work of Derwent and Middleton (1996), Dixon  
 426 et al. (2001) developed a new  $\text{NO}_X - \text{NO}_2$  relationship based on a larger dataset  
 427 collected across multiple sites:

$$\frac{C_{\text{NO}_2}}{C_{\text{NO}_X}} = a + b \log(C_{\text{NO}_X}) + c \log(C_{\text{NO}_X})^2 + d \log(C_{\text{NO}_X})^3 + e \log(C_{\text{NO}_X})^4. \quad (30)$$

428 where  $C_{\text{NO}_2}$  and  $C_{\text{NO}_X}$  are the concentration in ppb of  $\text{NO}_2$  and  $\text{NO}_X$ , respec-  
 429 tively, and the polynomial constants take the following values at urban sites:  
 430  $a = -3.08308$ ,  $b = +7.472477$ ,  $c = -5.11636$ ,  $d = +1.381938$ ,  $e = -0.12919$ .  
 431 For  $C_{\text{NO}_X} < 15$  ppb, one should use  $C_{\text{NO}_2}/C_{\text{NO}_X} = 0.60$ . The model is referred  
 432 as DDM model in the following.

433

434 The four models are applied in a quasi-steady approximation, therefore de-  
 435 scribing temporal evolution of all variables (meteorological, emissions, back-  
 436 ground concentration) as the succession of stationary states lasting 1 hour.

437

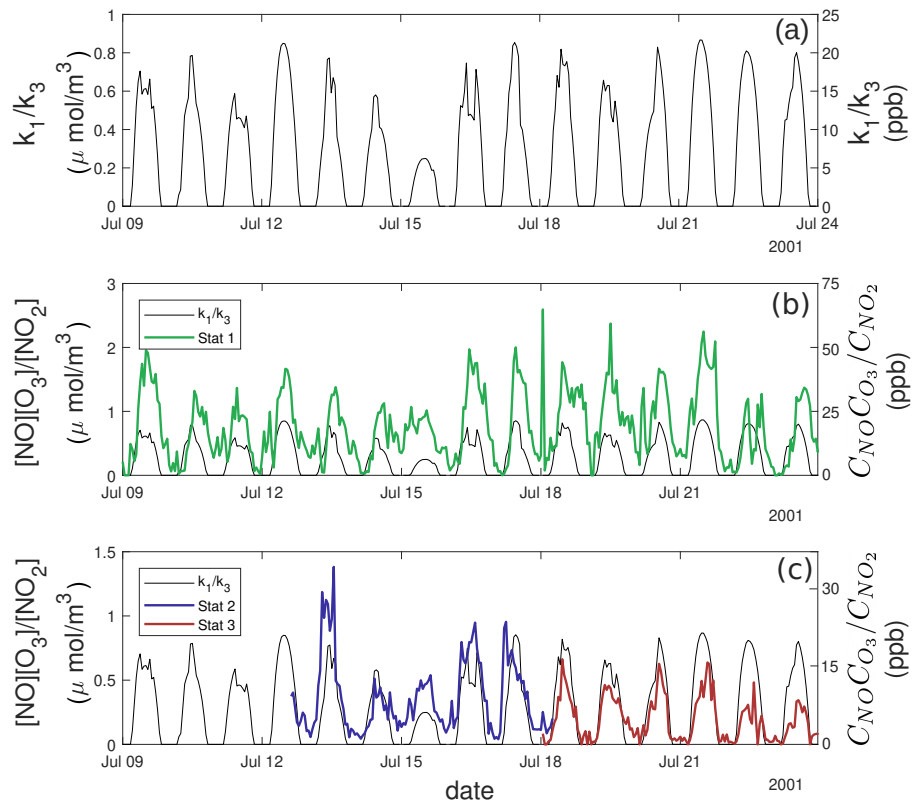


Figure 4: Evolution of the ratio  $k_1/k_3$  as predicted by Eq. 4 (a), and comparison with the ratio  $[\text{NO}][\text{O}_3]/[\text{NO}_2]$  in  $\mu\text{mol}/\text{m}^3$  ( $C_{\text{NO}}C_{\text{O}_3}/C_{\text{NO}_2}$  in ppb) for the site within the street canyon -Station 1- (b) and for the two sites in the courtyards -Station 2 and Station 3- (c).

	$k_1/k_3$ (ppb)	2	5	10	15	20	25
Relative variation of NO <sub>2</sub> concentration (%)	Station 1	14	8	Ref (0)	-7	-14	-20
	Station 2	18	11		-10	-19	-28
	Station 3	20	12		-11	-21	-31

Table 1: Sensitivity (e.g., relative variation of NO<sub>2</sub> concentration) of the output from Model 1 as a function of the ratio  $k_1/k_3$  (in ppb).

438 The simplest photostationary model (Model 1) assumes that the ratio  $k_1/k_3$   
439 is constant over time and for the different urban locations. According to Seinfeld  
440 (1986), we assume as a typical value for this ratio 10 ppb. This value is in line  
441 with the time average of the trend estimated by means of Eq. 4 and reported in  
442 Fig. 4.a. Moreover, we have tested the sensitivity of the model results to this  
443 constant by calculating the relative variation of the mean NO<sub>2</sub> concentration  
444 over the simulated period for different  $k_1/k_3$  ratios. The results are reported in  
445 Table 1. The concentration is very sensitive to variations in the ratio  $k_1/k_3$  and,  
446 as stated by Eq. 18, it increases as the ratio decreases. Moreover, the sensi-  
447 tivity of the model is higher for Station 2 and Station 3 with respect to Station 1.

448  
449 The results provided by the the three photo-chemical models are shown in  
450 Fig. 5, where measured and simulated NO<sub>2</sub> concentrations are plotted for the  
451 three monitoring stations. Moreover, following Chang and Hanna (2004), we  
452 assessed the performance of the models by means of multiple statistical indices:

- 453 • the Relative Error:  $RE = \left( \frac{2|C_m - C_p|}{C_m + C_p} \right)$ ;
- 454 • the Fractional Bias:  $FB = 2(\overline{C_m} - \overline{C_p}) / (\overline{C_m} + \overline{C_p})$ ;
- 455 • the Normal Mean Square Error:  $NMSE = \overline{(C_m - C_p)^2} / \overline{C_m C_p}$ ;
- 456 • the Mean Geometric bias:  $MG = \exp[\overline{\ln(C_m)} - \overline{\ln(C_p)}]$ ;
- 457 • the Geometrical mean squared Variance:  $VG = \exp[\overline{\ln(C_m) - \ln(C_p)^2}]$ ;
- 458 • the correlation coefficient:  $R = \frac{\overline{(C_m - \overline{C_m})(C_p - \overline{C_p})}}{\sigma_{C_m} \sigma_{C_p}}$ ;
- 459 • the ‘fraction in a factor of 2’: fraction of the data for which  $0.5 \leq C_p/C_m \leq$   
460 2,

461 where  $C_m$  and  $C_p$  are the measured and predicted concentrations, and  $\sigma_{C_m}$  and  
462  $\sigma_{C_p}$  their standard deviations. A perfect model would have MG, VG, R and  
463 FAC2=1, and FB, NMSE=0. A positive(negative) FB indicates that the model  
464 tends to underpredict(overpredict) the measures. Following Chang and Hanna  
465 (2004), the performances of a dispersion model can be defined as ‘good’ when  
466 the following criteria are satisfied:  $|\text{FB}| \leq 0.3$ ,  $\sqrt{\text{NMSE}} \leq 2$ ,  $0.7 \leq \text{MG} \leq 1.3$ ,  
467  $\text{VG} \leq 1.6$ ,  $\text{FAC2} \geq 0.5$ . In Hanna and Chang (2012), the same authors suggest  
468 a relaxation of these thresholds for application in urban areas. While all the  
469 statistical indices are used to assess the performance of the four models, we  
470 recall that only the correlation coefficient  $R$  is used as a criterion to uniquely  
471 determine the value  $\tau_s$  that maximizes the correlation between the results of the  
472 non-photostationary model (Model 3) and the experimental data (see Section  
473 1.4).

474

475 Panel a in Fig. 5 compares the measured and predicted concentrations for  
476 Station 1, which corresponds to the busy urban canyon with vehicular emissions.  
477 The photostationary model with constant  $k_1/k_3$  (Model 1) predicts with a good  
478 approximation the measured data but tends to overestimate  $\text{NO}_2$  for mean to  
479 high concentration values. This is confirmed by the negative fractional bias in  
480 Table 3. This overestimation is also observed for low concentrations when a  
481 variable  $k_1/k_3$  ratio is implemented in the photostationary model (Model 2).  
482 The slight loss of performance of Model 2 compared to Model 1 is highlighted  
483 by the statistical metrics in Table 3, with the increase in the absolute value of  
484 the fractional bias and the decrease in MG from 0.91 to 0.84. On the other  
485 hand, a noticeable improvement in the prediction is observed by applying the  
486 non-photostationary model (Model 3). The value of  $\tau_s$  that maximizes the  
487 correlation coefficient  $R$  is found to be equal to 89 s. This value is comparable  
488 with the time scale of the chemical reactions and thus confirms the need to adopt  
489 a non-photostationary solution (see Fig. 1). The scatter plot in Fig. 5 shows  
490 that the dispersion of the points around the bisector decreases with respect the  
491 photostationary models, as well as the relative error (RE) in Table 3. Finally, the

492 approach proposed by Dixon et al. (2001) (DDM model) fairly predicts low to  
493 medium concentrations but tends to cut the highest concentration values. The  
494 same trend was observed by Vardoulakis et al. (2007) by applying the model  
495 by Derwent and Middleton (1996), whose prediction is almost comparable to  
496 the DDM model for concentration up to 500 ppb. Vardoulakis et al. (2007)  
497 suggested that this underestimation of the  $\text{NO}_2$  concentration was because the  
498 empirical relationship was derived using measures that do not always reflect the  
499 typical  $\text{NO}_2/\text{NO}_x$  vehicle emission ratio of the case study.

500 Panels b and c in Fig. 5 compares the measured and predicted concentrations  
501 for Station 2 and 3, which correspond to the stations located within courtyards.  
502 Model 1 provides slightly scattered results and noticeably underestimates  $\text{NO}_2$   
503 concentration in Station 3 (FB=0.18 in Table 3). The adoption of a variable  
504  $k_1/k_3$  ratio (Model 2) improves the performance of the photostationary model.  
505 This is highlighted by the reduction in the relative error (RE), and by the  
506 trend towards 1 of the R metric. On the other hand, the adoption of the non-  
507 photostationary model (Model 3) does not bring further improvements. For both  
508 monitoring stations, the value of  $\tau_s$  that maximizes the correlation coefficient  
509  $R$  tends to infinity. As depicted in Fig. 1, this means that the results provided  
510 by the non-photostationary model ( $[\text{NO}_2]$ ) correspond to those provided by the  
511 photostationary one ( $[\text{NO}_2]^\infty$ ). This suggests that the pollutant concentrations  
512 in these sites already reached the photochemical equilibrium, as foreseen in Fig.  
513 4). Finally, the approach proposed by Dixon et al. (2001) performs worse than  
514 the three physically-based models also for Station 2 and 3. Differently from  
515 Station 1, here the predictions are significantly underestimated (FB=0.21 and  
516 0.28) also for low to medium concentration values.

517 Despite differences in performance, we finally notice that the statistical met-  
518 rics in Table 3 are within the validity ranges suggested by Chang and Hanna  
519 (2004) for all models.

520 In addition to  $\text{NO}_2$  concentrations, the models derived in Section 1 (and  
521 presented in Section 1.4) provide NO and  $\text{O}_3$  concentrations. Fig. 6 shows  
522 that, in a general way, the concentrations of NO are well simulated by the

		RE	FB	NMSE	MG	VG	R	FAC2
M1	Station 1	0.18	-0.12	0.05	0.91	1.01	0.96	1.00
	Station 2	0.13	0.04	0.03	1.06	1.00	0.94	1.00
	Station 3	0.17	0.18	0.07	1.18	1.03	0.96	1.00
M2	Station 1	0.18	-0.15	0.04	0.84	1.03	0.97	1.00
	Station 2	0.07	-0.05	0.02	0.95	1.00	0.97	1.00
	Station 3	0.10	0.10	0.02	1.09	1.01	0.99	1.00
M3	Station 1	0.09	0.00	0.01	1.01	1.00	0.99	0.99
	Station 2	0.07	-0.05	0.02	0.95	1.00	0.97	1.00
	Station 3	0.09	0.10	0.02	1.09	1.01	0.99	1.00
DDM	Station 1	0.21	0.05	0.09	1.04	1.00	0.86	1.00
	Station 2	0.27	0.21	0.08	1.29	1.07	0.93	1.00
	Station 3	0.32	0.28	0.12	1.38	1.11	0.96	1.00

Table 2: Performance statistics for the four investigated models (M1, M2, M3, DDM) in predicting the measured NO<sub>2</sub> concentration in the three measurement stations. Station 1 is to the busy street canyon, while Station 2 and 3 are courtyards.

523 proposed models. As observed for NO<sub>2</sub> concentrations, the non-photostationary  
524 model (Model 3) outperforms Model 2 for Station 1, while for Stations 2 and 3  
525 adopting the photostationary model with variable  $k_1/k_3$  is sufficient to maximize  
526 correlation. The DDM model shows good agreement for Station 1 for high  
527 concentration values, while for medium-low values (between 50 and 100 ppb)  
528 the error is significant. In accordance with Eq. 19, this behaviour reflects  
529 the results found for NO<sub>2</sub> concentrations. We also observe that for stations 2  
530 and 3, the DDM model fails to reproduce low NO concentrations. Regarding  
531 the prediction of ozone, the same considerations made for NO and NO<sub>2</sub> are  
532 valid: Model 3 brings significant improvements in results for the busy street  
533 canyon (Station 1), while the photostationary assumption (Model 2) holds when  
534 predicting concentrations in stations far from direct emissions (Station 2 and  
535 3).

#### 536 4. Conclusions

537 In this work we have derived different box models to simulate the concen-  
538 tration of NO, NO<sub>2</sub> and O<sub>3</sub> in a street canyon. Starting from a mass balance in  
539 the street, we have first defined a model for a passive tracer, then for chemical  
540 species at photostationary equilibrium and finally for the non-photostationary

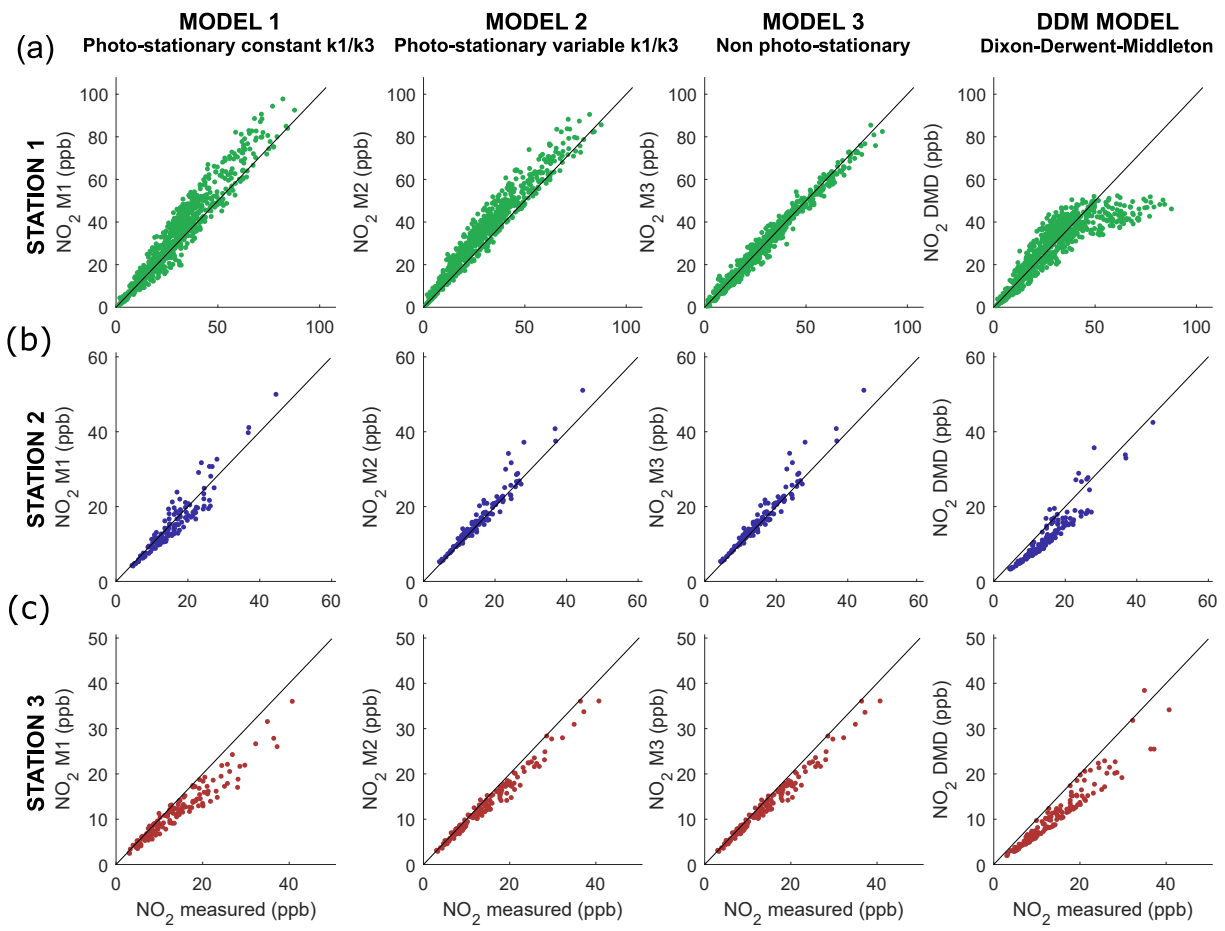


Figure 5: Comparison between the measured NO<sub>2</sub> concentrations in Station 1 (a), Station 2 (b) and Station 3 (c) against the concentrations computed with the three different photochemical models (M1, M2 and M3) and with the Derwent-Middleton model. Each point corresponds to one hour average concentration. Station 1 is to the busy street canyon, while Station 2 and 3 are courtyards.

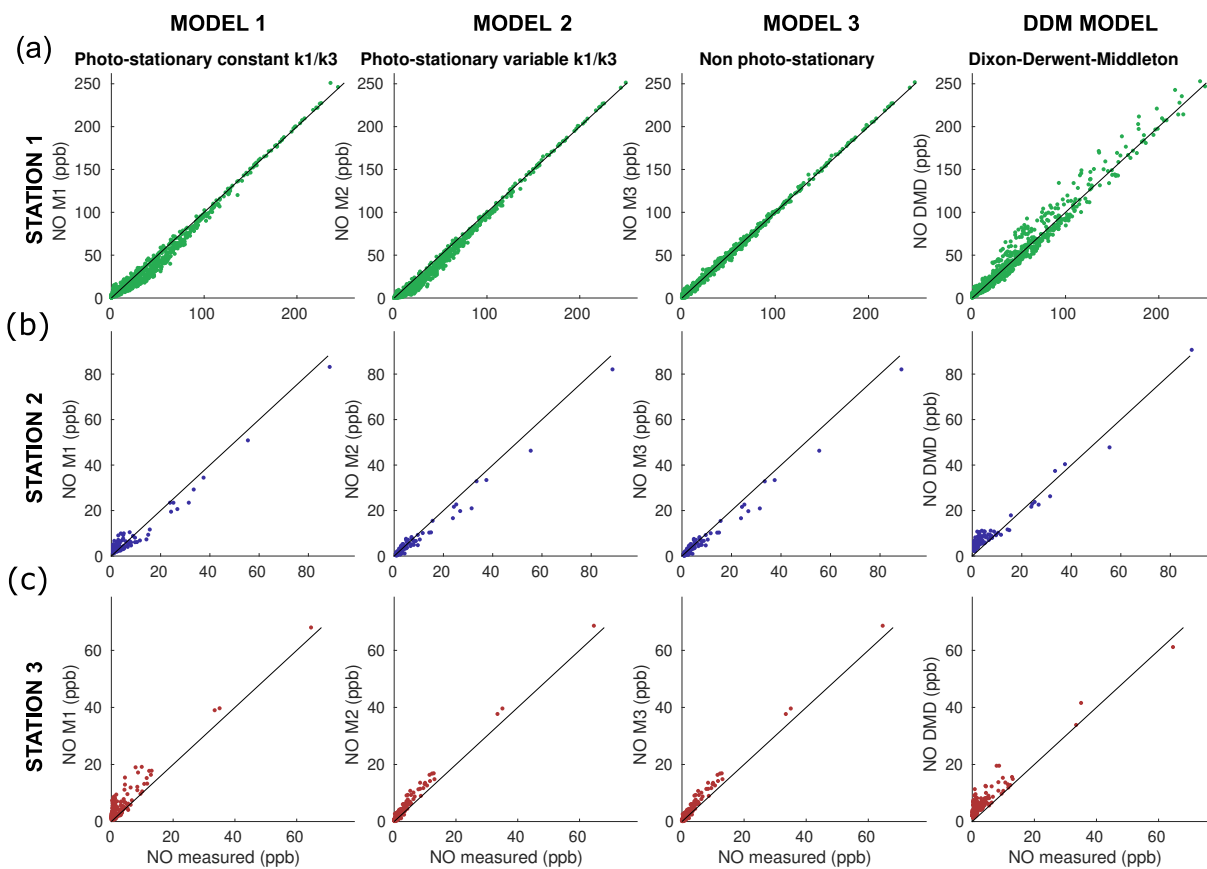


Figure 6: Comparison between the measured NO concentrations in Station 1 (a), Station 2 (b) and Station 3 (c) against the concentrations computed with the three different photochemical models (M1, M2 and M3) and with the Derwent-Middleton model. Each point corresponds to one hour average concentration. Station 1 is to the busy street canyon, while Station 2 and 3 are courtyards.

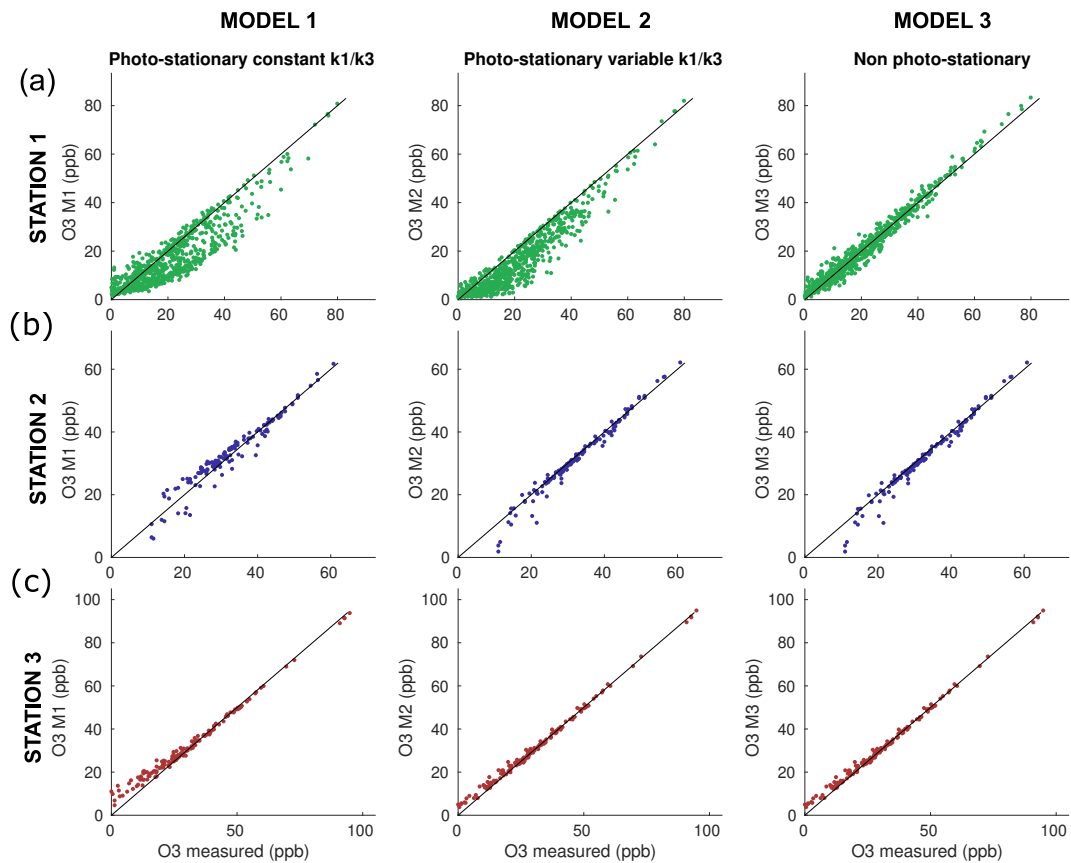


Figure 7: Comparison between the measured  $O_3$  concentrations in Station 1 (a), Station 2 (b) and Station 3 (c) against the concentrations computed with the three different photochemical models (M1, M2 and M3). Each point corresponds to one hour average concentration. Station 1 is to the busy street canyon, while Station 2 and 3 are courtyards.

541 state. Prediction from the simulations were compared with concentration mea-  
542 surements acquired during a field campaign. Results showed that the photosta-  
543 tionary models adequately reproduce the pollutant concentration in canyons far  
544 from direct vehicular emissions. However, the implementation of a parameteri-  
545 zation for the reaction rates according to the meteorological conditions is crucial.  
546 In busy streets, the photostationary equilibrium is not yet fully achieved and  
547 the non-photostationary model performs better. Finally, empirical models such  
548 as Dixon-Derwent-Middleton relationship fail to reproduce concentration peaks  
549 in busy canyons and underestimate  $\text{NO}_2$  concentrations at photochemical equi-  
550 librium. These results show that the photostationary model with meteorology-  
551 based parameters is satisfactory in reproducing the concentrations in different  
552 urban scenarios. However, the non-photostationary model brings significant  
553 improvements in busy street canyons.

554 Differently from previous studies, the chemical models presented here in-  
555 clude a description of the longitudinal and vertical ventilation processes and are  
556 therefore suitable for application to a network of streets with pollutant fluxes at  
557 street intersections. This paves the way for their implementation in operational  
558 street network models such as Sirane.

559 Furthermore, the adoption of a coherent formulation and the analysis of the  
560 balance equations in terms of characteristic transport and reaction times clarify  
561 the processes involved, the physico-chemical assumptions, and the limits of their  
562 validity. This information is critical to understanding, developing, and improv-  
563 ing the parametric models used in existing air quality simulation software. In  
564 this regard, a desirable development is the treatment of non-photostationarity  
565 outside the urban canopy, i.e. over rooftops or on high-emission roads in open  
566 terrain.

567 Finally, we notice that the diffusion of low-cost sensors provides nowadays  
568 large databases of pollutant concentration in cities. The inclusion of more accu-  
569 rate transport and reaction models in operational tools for urban air pollution  
570 is in line with this growing availability of data that can be used for validation  
571 and data assimilation. In this sense, this work highlights the feasibility of im-

572 plementing non-photostationary models in simulation tools at the city scale and  
573 paves the way for further application and validation.

## 574 **References**

- 575 Anenberg, S.C., Mohegh, A., Goldberg, D.L., Kerr, G.H., Brauer, M., Burkart,  
576 K., Hystad, P., Larkin, A., Wozniak, S., Lamsal, L., 2022. Long-term trends  
577 in urban  $no_2$  concentrations and associated paediatric asthma incidence: es-  
578 timates from global datasets. *The Lancet Planetary Health* 6, e49–e58.
- 579 Azzi, M., Johnson, G., Cope, M., 1992. An introduction to the generic reaction  
580 set photochemical smog mechanism .
- 581 Baik, J.J., Kang, Y.S., Kim, J.J., 2007. Modeling reactive pollutant dispersion  
582 in an urban street canyon. *Atmospheric Environment* 41, 934–949.
- 583 Baker, J., Walker, H.L., Cai, X., 2004. A study of the dispersion and transport  
584 of reactive pollutants in and above street canyons—a large eddy simulation.  
585 *Atmospheric Environment* 38, 6883–6892.
- 586 Berkowicz, R., Hertel, O., Larsen, S.E., Soerensen, N.N., Nielsen, M., 1997.  
587 Modelling traffic pollution in streets .
- 588 Bright, V.B., Bloss, W.J., Cai, X., 2013. Urban street canyons: Coupling dy-  
589 namics, chemistry and within-canyon chemical processing of emissions. *At-*  
590 *mospheric Environment* 68, 127–142.
- 591 Buccolieri, R., Gromke, C., Di Sabatino, S., Ruck, B., 2009. Aerodynamic  
592 effects of trees on pollutant concentration in street canyons. *Science of the*  
593 *Total Environment* 407, 5247–5256.
- 594 Carruthers, D., Edmunds, H., Lester, A., McHugh, C., Singles, R., 2000. Use  
595 and validation of ADMS-Urban in contrasting urban and industrial locations.  
596 *International Journal of Environment and Pollution* 14, 364–374.
- 597 CERC, 2022. ADMS technical specifications. URL:  
598 <http://www.cerc.co.uk/environmental-software/technical-specifications.html>.

- 599 Chang, J.C., Hanna, S.R., 2004. Air quality model performance evaluation.  
600 Meteorology and Atmospheric Physics 87, 167–196.
- 601 Derwent, R., Middleton, D., 1996. An empirical function for the ratio  $no_2: no_x$ .  
602 Clean Air 26, 57–60.
- 603 Dixon, J., Middleton, D., Derwent, R., 2001. Sensitivity of nitrogen dioxide con-  
604 centrations to oxides of nitrogen controls in the united kingdom. Atmospheric  
605 Environment 35, 3715–3728.
- 606 Fellini, S., Ridolfi, L., Salizzoni, P., 2020. Street canyon ventilation: Combined  
607 effect of cross-section geometry and wall heating. Quarterly Journal of the  
608 Royal Meteorological Society 146, 2347–2367.
- 609 Garmory, A., Kim, I., Britter, R., Mastorakos, E., 2009. Simulations of the dis-  
610 persion of reactive pollutants in a street canyon, considering different chemical  
611 mechanisms and micromixing. Atmospheric Environment 43, 4670–4680.
- 612 Hanna, S., Chang, J., 2012. Acceptance criteria for urban dispersion model  
613 evaluation. Meteorology and Atmospheric Physics 116, 133–146.
- 614 Hirtl, M., Baumann-Stanzer, K., 2007. Evaluation of two dispersion models  
615 (ADMS-Roads and LASAT) applied to street canyons in stockholm, london  
616 and berlin. Atmospheric Environment 41, 5959–5971.
- 617 Jenkin, M.E., Clemitshaw, K.C., 2000. Ozone and other secondary photochem-  
618 ical pollutants: chemical processes governing their formation in the planetary  
619 boundary layer. Atmospheric Environment 34, 2499–2527.
- 620 Kasten, F., Czeplak, G., 1980. Solar and terrestrial radiation dependent on the  
621 amount and type of cloud. Solar energy 24, 177–189.
- 622 Khreis, H., Kelly, C., Tate, J., Parslow, R., Lucas, K., Nieuwenhuijsen, M., 2017.  
623 Exposure to traffic-related air pollution and risk of development of childhood  
624 asthma: a systematic review and meta-analysis. Environment international  
625 100, 1–31.

- 626 Kim, M.J., Park, R.J., Kim, J.J., 2012. Urban air quality modeling with full o<sub>3</sub>-  
627 nox-voc chemistry: Implications for o<sub>3</sub> and pm air quality in a street canyon.  
628 *Atmospheric Environment* 47, 330–340.
- 629 Kwak, K.H., Baik, J.J., 2012. A CFD modeling study of the impacts of NO<sub>x</sub>  
630 and VOC emissions on reactive pollutant dispersion in and above a street  
631 canyon. *Atmospheric Environment* 46, 71–80.
- 632 Leighton, P., 1961. *Photochemistry of air pollution*. Academic Press.
- 633 Li, C.W., Brasseur, G.P., Schmidt, H., Mellado, J.P., 2021. Error induced by  
634 neglecting subgrid chemical segregation due to inefficient turbulent mixing  
635 in regional chemical-transport models in urban environments. *Atmospheric  
636 Chemistry and Physics* 21, 483–503.
- 637 Lovarelli, D., Conti, C., Finzi, A., Bacenetti, J., Guarino, M., 2020. Describing  
638 the trend of ammonia, particulate matter and nitrogen oxides: The role of  
639 livestock activities in northern Italy during Covid-19 quarantine. *Environ-  
640 mental research* 191, 110048.
- 641 Marucci, D., Carpentieri, M., 2019. Effect of local and upwind stratification on  
642 flow and dispersion inside and above a bi-dimensional street canyon. *Building  
643 and Environment* 156, 74–88.
- 644 McHugh, C., Carruthers, D., Edmunds, H., 1997. ADMS–Urban: an air quality  
645 management system for traffic, domestic and industrial pollution. *Interna-  
646 tional Journal of Environment and Pollution* 8, 666–674.
- 647 Misra, P., Takigawa, M., Khatri, P., Dhaka, S.K., Dimri, A., Yamaji, K., Ka-  
648 jino, M., Takeuchi, W., Imasu, R., Nitta, K., et al., 2021. Nitrogen oxides  
649 concentration and emission change detection during COVID-19 restrictions  
650 in north india. *Scientific reports* 11, 1–11.
- 651 Ntziachristos, L., Samaras, Z., Eggleston, S., Gorissen, N., Hassel, D., Hickman,  
652 A., et al., 2000. Copert iii. Computer Programme to calculate emissions from

- 653 road transport, methodology and emission factors (version 2.1), European  
654 Energy Agency (EEA), Copenhagen .
- 655 Palmgren, F., Berkowicz, R., Hertel, O., Vignati, E., 1996. Effects of reduction  
656 of NO<sub>x</sub> on the NO<sub>2</sub> levels in urban streets. *Science of the Total Environment*  
657 189, 409–415.
- 658 Ravina, M., Caramitti, G., Panepinto, D., Zanetti, M., 2022. Air quality and  
659 photochemical reactions: analysis of NO<sub>x</sub> and NO<sub>2</sub> concentrations in the  
660 urban area of turin, italy. *Air Quality, Atmosphere & Health* 15, 541–558.
- 661 Romberg, E., Bosinger, R., Lohmeyer, A., Ruhnke, R., Roth, E., 1996. N0-  
662 N02-Umwandlungsmodell fur die Anwendung bei Immissionsprognosen fur  
663 Kfz-abgase. *Gefahrstoffe-Reinhaltung Luft* 56 , 215–218.
- 664 Salizzoni, P., Marro, M., Soulhac, L., Grosjean, N., Perkins, R.J., 2011. Turbu-  
665 lent transfer between street canyons and the overlying atmospheric boundary  
666 layer. *Boundary-layer meteorology* 141, 393–414.
- 667 Salizzoni, P., Soulhac, L., Mejean, P., 2009. Street canyon ventilation and  
668 atmospheric turbulence. *Atmospheric Environment* 43, 5056–5067.
- 669 Seinfeld, J.H., 1986. *Atmospheric chemistry and physics of air pollution*. Cali-  
670 fornia, California Institute of Technology Pasadena .
- 671 Sillman, S., 1999. The relation between ozone, NO<sub>x</sub> and hydrocarbons in urban  
672 and polluted rural environments. *Atmospheric Environment* 33, 1821–1845.
- 673 Soulhac, L., Nguyen, C.V., Volta, P., Salizzoni, P., 2017. The model SIRANE for  
674 atmospheric urban pollutant dispersion. PART III: Validation against NO<sub>2</sub>  
675 yearly concentration measurements in a large urban agglomeration. *Atmo-  
676 spheric environment* 167, 377–388.
- 677 Soulhac, L., Perkins, R.J., Salizzoni, P., 2008. Flow in a street canyon for any  
678 external wind direction. *Boundary-Layer Meteorology* 126, 365–388.

- 679 Soulhac, L., Salizzoni, P., 2010. Dispersion in a street canyon for a wind direc-  
680 tion parallel to the street axis. *Journal of Wind Engineering and Industrial*  
681 *Aerodynamics* 98, 903–910.
- 682 Soulhac, L., Salizzoni, P., Cierco, F., Perkins, R., 2011. The model SIRANE  
683 for atmospheric urban pollutant dispersion; part i, presentation of the model.  
684 *Atmospheric environment* 45, 7379–7395.
- 685 Soulhac, L., Salizzoni, P., Mejean, P., Didier, D., Rios, I., 2012. The model  
686 SIRANE for atmospheric urban pollutant dispersion; PART II, validation of  
687 the model on a real case study. *Atmospheric environment* 49, 320–337.
- 688 Toscano, D., Murena, F., 2020. The effect on air quality of lockdown directives  
689 to prevent the spread of SARS-CoV-2 pandemic in Campania Region—Italy:  
690 indications for a sustainable development. *Sustainability* 12, 5558.
- 691 Vardoulakis, S., Valiantis, M., Milner, J., ApSimon, H., 2007. Operational air  
692 pollution modelling in the UK — Street canyon applications and challenges.  
693 *Atmospheric Environment* 41, 4622–4637.
- 694 Venkatram, A., Karamchandani, P., Pai, P., Goldstein, R., 1994. The develop-  
695 ment and application of a simplified ozone modeling system (SOMS). *Atmo-*  
696 *spheric Environment* 28, 3665–3678.
- 697 Yamartino, R.J., Wiegand, G., 1986. Development and evaluation of simple  
698 models for the flow, turbulence and pollutant concentration fields within an  
699 urban street canyon. *Atmospheric Environment (1967)* 20, 2137–2156.